A universal framework for non-deteriorating time-domain numerical algorithms in Maxwell's electrodynamics

A. Fedoseyev, E. J. Kansa, S. Tsynkov, S. Petropavlovskiy, M. Osintcev, U. Shumlak, and W. D. Henshaw

Citation: AIP Conference Proceedings **1773**, 020001 (2016); doi: 10.1063/1.4964955
View online: http://dx.doi.org/10.1063/1.4964955
View Table of Contents: http://scitation.aip.org/content/aip/proceeding/aipcp/1773?ver=pdfcov
Published by the AIP Publishing

A Universal Framework for Non-deteriorating Time-domain Numerical Algorithms in Maxwell's Electrodynamics

A. Fedoseyev[1,a),b)], E.J. Kansa[1], S. Tsynkov[2], S. Petropavlovskiy[2], M. Osintcev[2], U. Shumlak[3] and W.D. Henshaw[4]

[1]*Computational Sciences LLC, Madison, AL, USA*
[2]*North Carolina State University, Raleigh, NC, USA*
[3]*University of Washington, Seattle, WA, USA*
[4]*Rensselaer Polytechnical Institute, Troy, NY, USA*

[a)]Corresponding author: aif@comscis.com
[b)]URL: http://www.comscis.com

Abstract. We present the implementation of the Lacuna method, that removes a key difficulty that currently hampers many existing methods for computing unsteady electromagnetic waves on unbounded regions. Numerical accuracy and/or stability may deteriorate over long times due to the treatment of artificial outer boundaries. We describe a developed universal algorithm and software that correct this problem by employing the Huygens' principle and lacunae of Maxwell's equations.

The algorithm provides a temporally uniform guaranteed error bound (no deterioration at all), and the software will enable robust electromagnetic simulations in a high-performance computing environment. The methodology applies to any geometry, any scheme, and any boundary condition. It eliminates the long-time deterioration regardless of its origin and how it manifests itself. In retrospect, the lacunae method was first proposed by V. Ryaben'kii and subsequently developed by S. Tsynkov.

We have completed development of an innovative numerical methodology for high fidelity error-controlled modeling of a broad variety of electromagnetic and other wave phenomena. Proof-of-concept 3D computations have been conducted that convincingly demonstrate the feasibility and efficiency of the proposed approach. Our algorithms are being implemented as robust commercial software tools in a standalone module to be combined with existing numerical schemes in several widely used computational electromagnetic codes.

INTRODUCTION

It is, indeed, well-known that many methods used for the treatment of outer boundaries in computational electromagnetism (CEM) do not provide guaranteed error bounds, and their performance may deteriorate over long time intervals. The methods found susceptible to this undesirable phenomenon include not only PMLs (of both the original split type due to Bérenger [1, 2], as well as more recent unsplit PMLs [3, 4, 5]), see [6, 7, 8], but also some local low order artificial boundary conditions (ABCs), see [9, 10, 11], and others.[1]

Several approaches have been introduced in the literature aimed at reducing or removing the aforementioned long-time instabilities. Optimal local ABCs were obtained in [11] showing that their construction (the number of modes) is inevitably affected by the desired accuracy and the designed time interval, on which this accuracy must be sustained. The "stabilized" versions of Higdon's [16, 17] and Liao's [18, Sec. 6.5] boundary conditions offered an improved performance but did not eliminate the instability completely [9]. Furthermore, efforts to stabilize higher order ABCs were unsuccessful [19]. And when the stability is achieved, it often compromises the accuracy over the lower end of the frequency spectrum [20]. Local ABCs with an almost uniform long-time accuracy have been built in [21] based on complete plane wave expansions, but the geometry in [21] is limited to that of a half-space. Stabilization techniques for PMLs include changing the governing equations in the layer [7] and introducing frequency-shifted [22, 23, 24] or non-linear [25] PMLs. Many of these modifications may perform well computationally, but theoretically

[1]Nonlocal ABCs based on integral equations typically show good long-time accuracy [12, 13, 14], but they are often limited from the standpoint of geometry. For a general review of radiation boundary conditions for Maxwell's equations see [15].

Application of Mathematics in Technical and Natural Sciences
AIP Conf. Proc. 1773, 020001-1–020001-21; doi: 10.1063/1.4964955
Published by AIP Publishing. 978-0-7354-1431-0/$30.00

it is not clear whether the modified layer remains perfectly matched or absorbing, in particular, absorbing regardless of the frequency. On the other hand, the PML still remains very much problem specific.

Hereafter, we propose to develop ***a universal algorithm*** that would ***completely eliminate the long-time deterioration.*** It will be able to complement and "fix" any existing numerical scheme used for integrating the Maxwell equations inside the computational domain, as well as any existing procedure used for the treatment of the outer boundaries. The key idea is not to investigate the mechanism of deterioration in every case, but rather ***build a technique that would work even when this mechanism is not known.*** The resulting combined procedure will be ***completely general and will not require any specific information about the design or the parameters of the underlying ABC or PML.*** It will guarantee ***a non-deteriorating performance*** of the outer boundary for as long as the integration is conducted, regardless of either why the deterioration has originally occurred, or how it actually manifested itself.

Our algorithm relies on the Huygens' principle, *i.e.*, on the presence of secondary lacunae in the sense of Petrowsky [26] in the solutions of Maxwell's equations. Lacunae are the areas of "quietness" behind the aft (trailing) fronts of the waves. They characterize the propagation in odd dimensional spaces. Their opposite is the wave diffusion, which takes place in the spaces of even dimension, see, *e.g.*, [27, 28].

The question of identifying those hyperbolic equations and systems that admit the diffusionless propagation of waves has been first formulated by Hadamard [29, 30, 31]. He, however, did not know any other examples besides the scalar d'Alembert (wave) equation. The notion of lacunae was introduced and studied by Petrowsky in work [26], see also [28, Chapter VI]. He has obtained conditions for the coefficients of hyperbolic equations that guaranteed the existence of lacunae. Subsequent developments can be found in the work by Atiyah, Bott, and Gårding in [32, 33]. However, since work [26] no other constructive examples of either scalar equations or systems that satisfy the Huygens' principle have been found except for the wave equation and its equivalents. Specifically, Matthisson [34] has shown that in the standard 3 + 1-dimensional space-time with Minkowski metric, the only scalar hyperbolic equation that has lacunae is the d'Alembert equation. Later, Stellmacher [35, 36, 37] has built examples of nontrivial (*i.e.*, irreducible to the wave equation) diffusionless equations, but only in the spaces $\mathbb{R}^n$ for odd $n \geqslant 5$. Günther and his school have provided examples of nontrivial diffusionless systems (as opposed to scalar equations) in the standard Minkowski $3+1$ space-time [38, 39, 40], and examples of nontrivial scalar Huygens' equations in a $3+1$-dimensional space-time but equipped with a different metric (the so-called plane wave metric that contains off-diagonal terms), see [39, 40, 41]. Lax and Phillips have shown that the wave equation on the n-dimensional sphere, where $n \geqslant 3$ is odd, satisfies the Huygens' principle, see [42]; this spherical wave equation can be transformed to the Euclidean wave equation locally, but not globally.

As far as the Maxwell equations, the Huygens' principle applies either in its original or in the generalized form. The generalized Huygens' principle allows for a non-zero electrostatic solution instead of the identical zero behind the aft fronts, in which case we refer to quasi-lacunae as opposed to conventional lacunae [43]. The use of lacunae or quasi-lacunae enables a representation of the solution as the sum of a finite non-increasing number of terms so that each has only a finite non-increasing lifespan on the domain of interest. This immediately leads to a temporally uniform error estimate, *i.e.*, to the grid convergence that is uniform in time [44, 45, 46, 47]. When applied to a given ABC or a PML, the lacunae-based integration guarantees that the performance of the boundary condition will not deteriorate over arbitrarily long times [48, 49].

Our algorithm provides guaranteed error bounds for a broad range of time-dependent formulations that involve artificial boundaries. It applies to any existing numerical scheme used for integrating the Maxwell equations inside the computational domain, as well as to any existing procedure used for the treatment of the outer boundaries. It requires no problem-specific fine-tuning and thus facilitates high fidelity modeling for a variety of electromagnetic and other wave dominated phenomena.

Moreover, lacunae-based integration can provide a closure for the solution at the artificial outer boundary completely on its own, *i.e.*, without having to be coupled to an ABC or a PML [44, 45, 46, 47]. This may require a wider buffer region around the computational domain than an average PML would need. On the other hand, the shape of the artificial boundary in this case can be quite general, and the methodology will remain provably free from any error associated with the domain truncation.

- In practice, Fredholm *first kind integral equations* are commonly used despite their ill-posedness. An example is the electric field integral equation (EFIE) applied to perfect conductors [50, 51]. As there is a very strong and unambiguous emphasis in the solicitation on *guaranteed error bounds and guaranteed high fidelity modeling,* we are not planning to consider first kind equations, unless specifically requested.
- Ill-conditioning of the magnetic field integral equation (MFIE) with edges or corners [50, 51, 52].

- Spurious resonances of the magnetic field integral equation (MFIE). Can be alleviated by switching to the combined field integral equation (CFIE), a combination of MFIE and EFIE. However, EFIE leads to ill-conditioning, especially at low frequencies and for fine meshes (see item below), [53, 50, 51, 52, 54].
- The *low-frequency breakdown* of many computational methods that commonly manifests itself on fine meshes (with sizes $\leqslant$ wavelength). Its mathematical source is the degeneracy of the curl-curl operator in Maxwell's equations and, in EFIE, the presence of the hypersingular (grad-div) term, [50, 51, 55, 52, 56].

Our team, with its broad and extensive expertise in computational electromagnetism, is in an excellent position to address the items above, if so requested by the Army. We note in passing that satisfactory ways of dealing with these issues are already available in the literature (the loop-star decomposition of the basis, Calderon regularization, hierarchical preconditioners, and more), [53, 50, 51, 52, 54, 55, 56, 57, 58, 59, 60, 61].

TIME-MARCHING USING QUASI-LACUNAE OF MAXWELL'S EQUATIONS

The propagation of unsteady electromagnetic waves in vacuum is governed by time-dependent Maxwell's equations:

$$\frac{1}{c}\frac{\partial \mathbf{E}}{\partial t} - \operatorname{curl}\mathbf{H} = -\frac{4\pi}{c}\mathbf{j} \quad \text{and} \quad \frac{1}{c}\frac{\partial \mathbf{H}}{\partial t} + \operatorname{curl}\mathbf{E} = -\frac{4\pi}{c}\mathbf{j}^{\mathrm{M}}. \tag{1}$$

supplemented by the Gauss laws of electricity and magnetism:

$$\operatorname{div}\mathbf{E} = 4\pi\rho \quad \text{and} \quad \operatorname{div}\mathbf{H} = 4\pi\rho^{\mathrm{M}}. \tag{2}$$

The currents $\mathbf{j}$, $\mathbf{j}^{\mathrm{M}}$ and charges ρ, ρ^{M} that drive system (1)-(2)[2] are subject to the conservation requirement [62, 63]. The conservation of electric charge can be written in the form of the continuity equation:

$$\frac{\partial \rho}{\partial t} + \operatorname{div}\mathbf{j} = 0. \tag{3}$$

Then, the Gauss law of electricity shall be regarded as an implication of the Ampère law [first equation (1)] and the conservation requirement. The charge $\rho = \rho(\mathbf{x}, t)$ in (2) shall be interpreted as the charge accumulated between 0 and t due to the current $\mathbf{j}(\mathbf{x}, t)$. Similar conclusions hold for the magnetic part.

Straightforward transformations of Eqs. (1)-(2) lead to the vector d'Alembert equation for the electric field:

$$\frac{1}{c^2}\frac{\partial^2 \mathbf{E}}{\partial t^2} - \Delta\mathbf{E} = -4\pi\left[\frac{1}{c^2}\frac{\partial \mathbf{j}}{\partial t} + \frac{1}{c}\operatorname{curl}\mathbf{j}^{\mathrm{M}} + \operatorname{grad}\rho\right] \tag{4}$$

and a completely similar equation for the magnetic field: Let's now assume that $\mathbf{j}$ and $\mathbf{j}^{\mathrm{M}}$ are compactly supported in space-time on a bounded domain $Q \subset \mathbb{R}^3 \times [0, +\infty]$. If the right-hand sides (RHSs) of Eq. (4) and the corresponding magnetic equation were compactly supported as well, then the solutions $\mathbf{E}$ and $\mathbf{H}$ would have classical lacunae in the sense of Petrowsky [26]. However, due to the terms $\operatorname{grad}\rho$ and $\operatorname{grad}\rho^{\mathrm{M}}$, these RHSs may not vanish even as the currents $\mathbf{j}$ and $\mathbf{j}^{\mathrm{M}}$ cease to operate. This corresponds to the accumulation of charges, see Eq. (3). Then, as we have shown in [43], instead of the classical lacunae the solutions $\mathbf{E} = \mathbf{E}(\mathbf{x}, t)$ and $\mathbf{H} = \mathbf{H}(\mathbf{x}, t)$ *will have quasi-lacunae*:

$$\mathbf{E} = \mathbf{E}^{\mathrm{st}},\ \mathbf{H} = \mathbf{H}^{\mathrm{st}}\ \ \forall\, \mathbf{x}, t \in \bigcap_{(\boldsymbol{\xi},\tau)\in Q} \{(\mathbf{x}, t)\,|\,|\mathbf{x} - \boldsymbol{\xi}| < c\,(t - \tau)\,,\ t > \tau\}. \tag{5}$$

In formula (5), $\mathbf{E}^{\mathrm{st}} = \mathbf{E}^{\mathrm{st}}(\mathbf{x})$ and $\mathbf{H}^{\mathrm{st}} = \mathbf{H}^{\mathrm{st}}(\mathbf{x})$ are the electrostatic and magnetostatic fields due to the accumulated electric and magnetic charges $\rho = \rho(\mathbf{x})$ and $\rho^{\mathrm{M}} = \rho^{\mathrm{M}}(\mathbf{x})$. They satisfy the Poisson equations:

$$\Delta\mathbf{E}^{\mathrm{st}} = 4\pi\operatorname{grad}\rho \quad \text{and} \quad \Delta\mathbf{H}^{\mathrm{st}} = 4\pi\operatorname{grad}\rho^{\mathrm{M}}, \tag{6}$$

respectively. In addition, $\mathbf{E}^{\mathrm{st}}$ and $\mathbf{H}^{\mathrm{st}}$ would have vanished if they were to extend all the way to infinity. Formulae (5) and (6) can be proven by analyzing the Kirchhoff integral, and showing that inside the lacuna it reduces to the classical Newton's volume potential [43].

[2] The magnetic charge ρ^{M} and current $\mathbf{j}^{\mathrm{M}}$ do not exist in nature and are introduced only for the convenience of analysis.

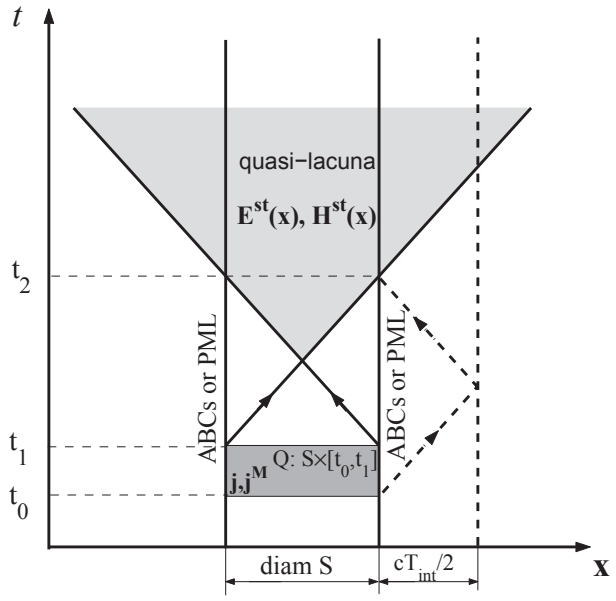

FIGURE 1. Quasi-lacuna is the common interior or all forward light cones when the vertex sweeps the support of the RHS. Inside is the electrostatic (and magnetostatic) solution due to the accumulated charges

Let $S \subset \mathbb{R}^3$ be a bounded computational domain, and let $\mathbf{j}$ and $\mathbf{j}^{\mathrm{M}}$ be compactly supported on $Q = \{(\mathbf{x}, t)\,|\mathbf{x} \in S,\ t_0 < t < t_1\}$, see Figure 1, so that on $\mathbb{R}^3 \backslash S$ the Maxwell equations are homogeneous. Our objective is to compute $\mathbf{E}$ and $\mathbf{H}$ only on S, while truncating its unbounded complement and replacing it by an ABC or a PML at the outer boundary ∂S. Note that by the time $t_2 = t_0 + \frac{1}{c}\mathrm{diam}\, S + t_1 - t_0 \stackrel{\mathrm{def}}{=} t_0 + T_{\mathrm{int}}$ the domain S will completely fall into the quasi-lacuna (5), and will remain there for all $t > t_2$. In other words, once the currents ceases to operate (at $t = t_1$), it takes an additional $\frac{1}{c}\mathrm{diam}\, S$ "seconds" for the waves to leave the domain S. Consequently, we can integrate (1) on the finite interval T_{int} using any appropriate scheme, and then stop because at $t_2 = t_0 + T_{\mathrm{int}}$ the solution on S reaches its steady state and no longer evolves. If we use an ABC or a PML, then no adverse phenomenon, such as an instability will be able to manifest itself provided that the interval T_{int} is not too long.

Let the currents in (1) operate continuously for $0 < t < +\infty$ and partition them into the intervals T_0:

$$\mathbf{j}(\mathbf{x}, t) = \sum_{i=0}^{\infty} \mathbf{j}_i(\mathbf{x}, t), \quad \mathbf{j}_i(\mathbf{x}, t) = \begin{cases} \mathbf{j}(\mathbf{x}, t), & iT_0 \leqslant t < (i+1)T_0, \\ 0, & \text{otherwise}, \end{cases} \tag{7}$$

and similarly for the magnetic field. Then, each system (1) driven by the RHS ((7)) for a particular i (a partial subproblem) will have a quasi-lacuna, and as such, can be integrated independently from $t_0^{(i)} \stackrel{\mathrm{def}}{=} iT_0$ to $t_2^{(i)} \stackrel{\mathrm{def}}{=} t_0^{(i)} + T_{\mathrm{int}} = t_0^{(i)} + T_0 + \frac{1}{c}\mathrm{diam}\, S$. At $t_2^{(i)}$, its solution reaches the steady state on the domain of interest S. Hence, it does not need to be advanced any further. The overall solution can subsequently be obtained by linear superposition. If each partial subproblem is terminated by an ABC or a PML at ∂S, then no negative effect due to this ABC or PML will manifest itself provided that the integration interval $T_{\mathrm{int}} = T_0 + \frac{1}{c}\mathrm{diam}\, S$ is not excessively long.

Time-marching of the overall solution requires summation of the individual contributions for $i = 0, 1, 2, \ldots$. However, the causality principle implies that for any t, no portion of the RHS (7) that corresponds to later times can contribute to the solution. Therefore, the summation will terminate at $N_1 \stackrel{\mathrm{def}}{=} \lceil t/T_0 \rceil - 1$, where $\lceil t/T_0 \rceil$ is the smallest integer $\geqslant t/T_0$. Otherwise, there will be steady and unsteady terms in the sum. The unsteady terms $\mathbf{E}_i(\mathbf{x}, t)$ and $\mathbf{H}_i(\mathbf{x}, t)$, $i = N_0, \ldots, N_1$, [solutions of (1) (7)] are those that have not reached their steady state on S yet. The index N_0 corresponds to the last term, counting backwards, for which S is not completely inside the quasi-lacuna yet; $N_0 = \left\lceil \frac{t - \mathrm{diam}\, S/c}{T_0} \right\rceil$. The steady-state terms $\mathbf{E}^{\mathrm{st}}_{N_0}(\mathbf{x})$ and $\mathbf{H}^{\mathrm{st}}_{N_0}(\mathbf{x})$ are generated by the charges accumulated over the period $0 < t < N_0 T_0$, *i.e.*, for the operational time of the first N_0 partial sources (7), $i = 0, \ldots, N_0 - 1$. Altogether, we can thus

write:

$$\mathbf{E}(\mathbf{x},t) = \mathbf{E}^{\mathrm{st}}_{N_0}(\mathbf{x}) + \sum\nolimits_{i=N_0}^{N_1} \mathbf{E}_i(\mathbf{x},t), \tag{8}$$

and a similar expression for the magnetic field. It is very important that the number of unsteady terms on the RHS of Eq. (8) remains bounded for all times: $N_1 - N_0 + 1 \leqslant \left[\frac{\operatorname{diam} S/c}{T_0}\right] + 2$.

Since the charges are given functions of $\mathbf{x}$ and t, the fields $\mathbf{E}^{\mathrm{st}}_{N_0}(\mathbf{x})$ and $\mathbf{H}^{\mathrm{st}}_{N_0}(\mathbf{x})$ can be evaluated by solving the Poisson equations:

$$\Delta\varphi = -4\pi\rho \quad \text{and} \quad \Delta\varphi^{\mathrm{M}} = -4\pi\rho^{\mathrm{M}}, \tag{9}$$

at $t = N_0 T_0$, subject to $|\varphi| \to 0$ and $|\varphi^{\mathrm{M}}| \to 0$ as $|\mathbf{x}| \to \infty$, and then taking the anti-gradient of the potentials φ and φ^{M} on S, which will obviously yield the fields that satisfy (6). Thus, the steady-state solution is updated at those moments of time when the corresponding partial sources cease, *i.e.*, at $t = iT_0$.

A TEMPORALLY UNIFORM ERROR BOUND

In matrix notation, Maxwell's equations (1) along with the initial conditions can be written as

$$\begin{aligned} &\frac{1}{c}\frac{\partial \mathbf{w}}{\partial t} + \hat{\mathbf{L}}\mathbf{w} = \mathbf{f}(\mathbf{x},t), \quad \mathbf{x} \in \mathbb{R}^3,\ t > 0, \\ &\mathbf{w}(\mathbf{x},0) = \boldsymbol{\varphi}(\mathbf{x}), \quad \mathbf{x} \in \mathbb{R}^3, \end{aligned} \tag{10}$$

where $\mathbf{w} = [\mathbf{E},\mathbf{H}]^T$ is the vector of field components, $\hat{\mathbf{L}} = \begin{bmatrix} 0 & -\operatorname{curl} \\ \operatorname{curl} & 0 \end{bmatrix}$, $\boldsymbol{\varphi}(\mathbf{x})$ is the initial data, and $\mathbf{f}(\mathbf{x},t) = \left[-4\pi\mathbf{j}(\mathbf{x},t)/c, -4\pi\mathbf{j}^{\mathrm{M}}(\mathbf{x},t)/c\right]^T$. Both $\boldsymbol{\varphi}(\mathbf{x})$ and $\mathbf{f}(\mathbf{x},t)$ are assumed compactly supported in space, so that the far field part of problem (10) is homogeneous. To solve (10) on the computer, we choose a bounded computational domain S such that $\operatorname{supp}\boldsymbol{\varphi} \subset S$ and $\operatorname{supp}\mathbf{f} \subset S$, and set an ABC or PML $\hat{\boldsymbol{\Gamma}}$ at ∂S:

$$\begin{aligned} &\frac{1}{c}\frac{\partial \mathbf{w}^{(S)}}{\partial t} + \hat{\mathbf{L}}\mathbf{w}^{(S)} = \mathbf{f}(\mathbf{x},t), \quad \mathbf{x} \in S,\ t > 0, \\ &\hat{\boldsymbol{\Gamma}}\mathbf{w}^{(S)}(\mathbf{x},t) = \mathbf{0}, \quad \mathbf{x} \in \partial S,\ \ t > 0, \\ &\mathbf{w}^{(S)}(\mathbf{x},0) = \boldsymbol{\varphi}(\mathbf{x}), \quad \mathbf{x} \in S. \end{aligned} \tag{11}$$

In the case of an ABC, the operator $\hat{\boldsymbol{\Gamma}}$ specifies certain relations between the field components and, perhaps, their derivatives. In the case of a PML, $\hat{\boldsymbol{\Gamma}}$ may not have an explicit definition. However, for our purposes it is sufficient to assume that the relations enforced by $\hat{\boldsymbol{\Gamma}}$ are equivalent to having a specific PML outside ∂S.

An ideal ABC or PML would guarantee that the solutions of problems (10) and (11) coincide for $\mathbf{x} \in S$ and any $t > 0$: $\mathbf{w}(\mathbf{x},t) \equiv \mathbf{w}^{(S)}(\mathbf{x},t)$. In practice, however, we would expect that the following inequality holds:

$$\|\mathbf{w}(\mathbf{x},t) - \mathbf{w}^{(S)}(\mathbf{x},t)\| \leqslant \delta(\hat{\boldsymbol{\Gamma}}), \quad \mathbf{x} \in S. \tag{12}$$

The constant δ on the RHS of (12) depends on the operator $\hat{\boldsymbol{\Gamma}}$, *i.e.*, on the quality of the ABCs [64, 65, 66] or PML at ∂S. A non-deteriorating long-time performance implies, however, that δ does not depend on time, or more precisely, remains bounded as the time elapses. As indicated in Section b) though, this may not be the case either. The following Theorem was proven in [49] (see also [48] for an earlier version):

Theorem 1 *Let $S \subset \mathbb{R}^3$ be a bounded computational domain, and let problem (10) be solved on S using an appropriate ABC or PML that reduces it to problem (11). Let problem (11) be time marched with the help of quasi-lacunae (as described in Section b)). Let $[\boldsymbol{\mu}_i, \boldsymbol{\epsilon}_i, \boldsymbol{\xi}_i]$ be the perturbations of the RHS, boundary data, and initial data for the i-th partial problem of type (11), and let ψ be the perturbations of the data in the steady-state equations (9). Then, assuming that $\sup_i \|[\boldsymbol{\mu}_i, \boldsymbol{\epsilon}_i, \boldsymbol{\xi}_i]\|' < \infty$ and $\|\boldsymbol{\psi}\|'' < \infty$, the error on the computational domain S will remain uniformly bounded for all times:*

$$\|\tilde{\mathbf{w}}^{(S)}(\mathbf{x},t) - \mathbf{w}(\mathbf{x},t)\| \leqslant \delta(\hat{\boldsymbol{\Gamma}}) + C_1 \sup_i \|[\boldsymbol{\mu}_i, \boldsymbol{\epsilon}_i, \boldsymbol{\xi}_i]\|' + C_2\|\boldsymbol{\psi}\|''. \tag{13}$$

Theorem 1 guarantees that regardless of what causes the original long-time deterioration, time-marching with the help of quasi-lacunae will prevent any possible error growth.

APPLICATION TO NON-HUYGENS' PROBLEMS

From the standpoint of applications though, the key problem of interest is typically more involved:

$$\begin{aligned}
&\hat{\mathbf{F}}\left(\mathbf{x}, t, \mathbf{w}, \frac{\partial \mathbf{w}}{\partial t}, \frac{\partial \mathbf{w}}{\partial \mathbf{x}}, \ldots\right) = \mathbf{0}, \quad \mathbf{x} \in S,\ t > 0, \\
&\frac{1}{c}\frac{\partial \mathbf{w}}{\partial t} + \hat{\mathbf{L}}\mathbf{w} = \mathbf{0}, \quad \mathbf{x} \in \mathbb{R}^3 \backslash S,\ t > 0, \\
&\mathbf{w}(\mathbf{x}, 0) = \mathbf{0}, \quad \mathbf{x} \in \mathbb{R}^3 \backslash S.
\end{aligned} \tag{14}$$

In formula (14), the generic notation $\hat{\mathbf{F}}(\cdots)$ accounts for processes inside S, *e.g.*, the generation of fields by currents, scattering off shapes, lossy and/or dispersive media, nonlinear effects, *etc.* At the same time, the far-field solution is supposed to be governed by the constant coefficient homogeneous Maxwell equations, so that the operator $\hat{\mathbf{L}}$ in (14) is the same as in (10). The overall problem (14) is assumed uniquely solvable.

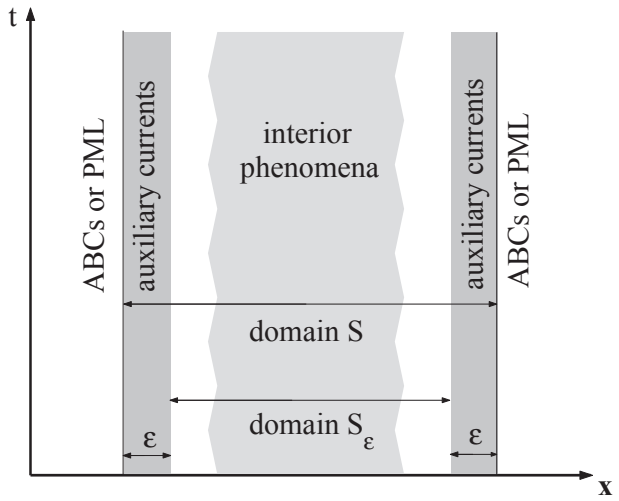

FIGURE 2. Computational setup. The phenomena of interest are inside S, outside is the free space, which is truncated off and replaced with an ABC or a PML. The auxiliary sources are in a narrow region of width ε right next to ∂S on the inside

Numerically, the far field is truncated and replaced by an ABC or a PML at ∂S, and we need to make sure that the performance of this ABC or PML does not deteriorate over long time intervals. To apply the method of Sections b) and b), we first decompose problem (14) into the interior and auxiliary problems (AP), see [44, 45, 46, 47]. The interior problem is posed on S for the same equation as in (14), and at ∂S we simply require that its solution coincide with the solution $\mathbf{w}^{\text{aux}}(\mathbf{x}, t)$ of the AP. The AP, in turn, is formulated on the entire space $\mathbb{R}^3$ as pure Maxwell's equations subject to the homogeneous initial conditions:

$$\begin{aligned}
&\frac{1}{c}\frac{\partial \mathbf{w}^{\text{aux}}}{\partial t} + \hat{\mathbf{L}}\mathbf{w}^{\text{aux}} = \mathbf{f}^{\text{aux}}(\mathbf{x}, t), \quad \mathbf{x} \in \mathbb{R}^3,\ t > 0, \\
&\mathbf{w}^{\text{aux}}(\mathbf{x}, 0) = \mathbf{0}, \quad \mathbf{x} \in \mathbb{R}^3.
\end{aligned} \tag{15}$$

Its solution is driven by the auxiliary electric and magnetic currents $\mathbf{f}^{\text{aux}}(\mathbf{x}, t) = -\frac{4\pi}{c}\left[\mathbf{j}, \mathbf{j}^{\text{M}}\right]^T$ that link the interior and the auxiliary problems and are constructed as follows.

Let $\mathbf{w}(\mathbf{x}, t)$ be the solution to (14). Consider a smooth scalar function $\mu(\mathbf{x})$, which satisfies $\mu(\mathbf{x}) \equiv 1$ for $\mathbf{x} \in \mathbb{R}^3 \backslash S$ and $\mu(\mathbf{x}) \equiv 0$ for $\mathbf{x} \in S_\varepsilon = \{\mathbf{x} | \mathbf{x} \in S,\ \text{dist}(\mathbf{x}, \partial S) > \varepsilon\}$, so that in a narrow region of width ε next to ∂S it undergoes a smooth transition from zero to one, see Figure 2.

Then, we multiply $\mathbf{w}(\mathbf{x}, t)$ by $\mu(\mathbf{x})$ and apply the full left-hand side operator of Maxwell's system ((10)) to this

product everywhere on $\mathbb{R}^3$ for all $t > 0$. This yields the RHS to the AP (15):

$$\mathbf{f}^{\text{aux}}(\mathbf{x}, t) \stackrel{\text{def}}{=} \frac{1}{c}\frac{\partial \mu \mathbf{w}}{\partial t} + \hat{\mathbf{L}}\mu\mathbf{w}. \tag{16}$$

Obviously, $\mathbf{f}^{\text{aux}} = \mathbf{0}$ for $\mathbf{x} \in S_\varepsilon \cup \mathbb{R}^3 \backslash S$ and any $t > 0$. The only region where $\mathbf{f}^{\text{aux}}$ may differ from zero is the transition region $S \backslash S_\varepsilon$.

Due to the unique solvability of Maxwell's equations, the solution $\mathbf{w}^{\text{aux}}(\mathbf{x}, t)$ to the AP ((15)) driven by $\mathbf{f}^{\text{aux}}$ of (16) coincides with the solution to ((14)) everywhere on $\mathbb{R}^3 \backslash S$ for all $t > 0$. Therefore, we can use $\mathbf{w}^{\text{aux}}$ to supply the required boundary data to the interior problem, and thus expect that its solution $\mathbf{w}(\mathbf{x}, t)$ will coincide with the solution of ((14)) inside S for all $t > 0$. The AP (15) is still formulated on an unbounded region. It is solved AP on the same bounded domain S, see Figure 2, using the same ABC or PML at ∂S that we would have used for the original problem (14). The key benefit of the decomposition is that the AP satisfies the (generalized) Huygens' principle. Therefore, we can integrate the AP using quasi-lacunae and thus guarantee the non-deteriorating performance of any appropriate ABC or PML. The block diagram of the overall algorithm is presented in Figure 2.

IMPLEMENTATION AND NUMERICAL RESULTS

Performance of the Various ABCs/PMLs Combined with Lacunae-based Time Marching

We have implemented the algorithm of Section b) in a flexible C++ software tool, using OpenMP for fast parallel computations, to demonstrate the efficiency and universality of the proposed lacunae-based methodology, and to conduct the study of performance of the various ABCs/PMLs combined with lacunae-based time marching.

Example test case presents a full 3D Cartesian setting for the computational domain shaped as a parallelepiped. At its outer surface the grid was terminated by the unsplit PML due to Zhao and Cangellaris [68]. Inside the computational domain, the governing equations were discretized on a uniform grid with square cells using the well-known second order accurate Yee scheme [69].

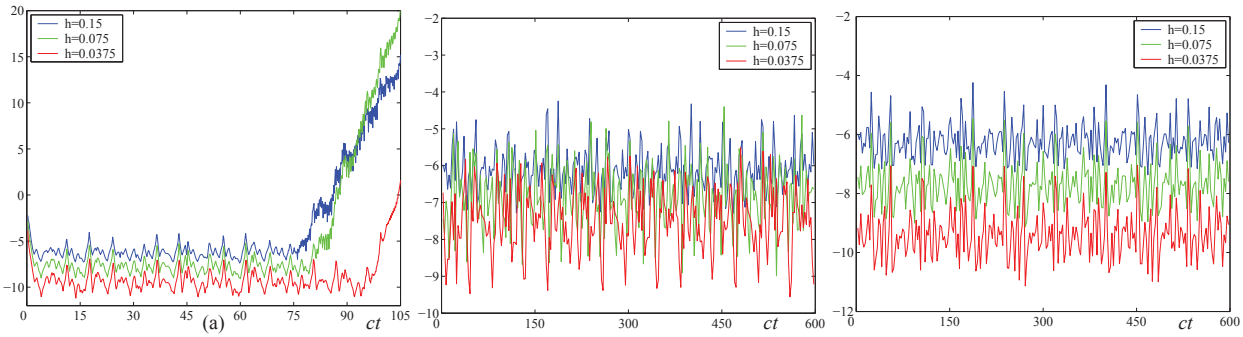

FIGURE 3. Results of computations. Binary logarithm of the error (L_∞ norm) *vs.* time on three successively refined grids shown by three different colors. Wiggles are due to the oscillatory nature of the solution itself. (a) PML — abrupt error buildup after some time elapses; (b) 1st order ABC — no error buildup and no grid convergence either because of large reflections; (c) PML+lacunae — no error buildup and 2nd order grid convergence (design rate)

In Figure 3, we are showing the profiles of the error (L_∞ norm) as it depends on time on three successively refined computational grids. Figure 3(a) clearly demonstrates that if the PML [68] is used to terminate the computational domain on its own, then after a certain period of "calm" the error starts to build up abruptly. Figure 3(b) corresponds to the PML switched off and the domain terminated by the local first order ABC:

$$\mathbf{H} = \mathbf{n} \times \mathbf{E}. \tag{17}$$

ABC (17) is designed to absorb the transverse plane waves traveling normal to the boundary; it is also used to terminate the PML at its outer boundary. As the only difference between the computations in Figure 3(a) and 3(b) is the PML,

we can unambiguously attribute the error growth shown in Figure 3(b) to the presence of the latter. At the same time, we notice that there is no long-time error growth in Figure 3(b). This indicates the the ABC (17) itself is apparently not prone to the deterioration of performance. However, it halts the grid convergence, because the accuracy of the boundary procedure is insufficient, and on fine grids the solution inside the computational domain is dominated by reflections from the outer boundary.

At the same time, Figure 3(c) clearly demonstrates that if the use of the PML is supplemented by the time-marching based on quasi-lacunae, then the long-time growth of the error is completely eliminated, yet the grid convergence with the design rate for the scheme, $O(h^2)$, is restored.

Low-order ABS Performance

A number of low-order ABS have been also tested and described below.

Sommerfeld Boundary Condition

Sommerfeld radiation boundary condition in the time domain is the simplest possible ABC. It is given by the following first order hyperbolic PDE:

$$\frac{\partial E}{\partial x} = \frac{1}{c}\frac{\partial E}{\partial t}. \tag{18}$$

Boundary condition (18) is transparent for the outgoing plane waves of the type $E = E(x - ct)$ traveling along the x axis in the positive direction toward the artificial boundary $x = \text{const}$. For other boundaries, such as $y = \text{const}$ and $z = \text{const}$, Sommerfeld boundary conditions are formulated similarly.

In all the cases, they are designed to absorb the waves at the normal incidence only. That's why it is expected that this boundary condition will produce a significant overall reflection error.

Higdon ABC

In work [17], Higdon has proposed a differential annihilator for the sum of N plane waves:

$$\prod_{n=1}^{N}\left(\cos\phi_n\frac{\partial}{\partial t} - c\frac{\partial}{\partial x}\right)E = 0. \tag{19}$$

Boundary condition (19) is exact for the plane waves traveling at the angles of incidence ϕ_n, $-\pi/2\phi_n < \pi/2$, toward the artificial boundary $x = \text{const}$. The order of the Higdon boundary operator is determined by the number of angles N. The second-order case, $N = 2$, of the Higdon boundary condition (19) has been implemented into our in-house code.

Betz-Mittra ABC

When an electromagnetic wave is interacting with an artificial outer boundary, both propagating and evanescent waves may get scattered. The Higdon ABC (19) is designed to annihilate the propagating waves, but is deficient in absorbing the evanescent waves. To circumvent this problem, Betz and Mittra in work [74, 75] have proposed a modified form of the Higdon ABC that also annihilates the evanescent waves:

$$\left(\frac{\partial}{\partial t} - \frac{c}{\cos\phi_1}\frac{\partial}{\partial x} + \alpha_1\right)\left(\frac{\partial}{\partial t} - \frac{c}{\cos\phi_2}\frac{\partial}{\partial x}\right)E = 0. \tag{20}$$

Boundary condition (20) is of second order; other orders can also be considered. The quantity α_1 in (20) is the attenuation constant chosen so that $\alpha_1\Delta x = 0.1$, where Δx is the grid size. A similar attenuation constant can also be introduced into the second factor of the operator on the left-hand side of (20). Boundary condition (20) has been implemented into our in-house code. For boundary conditions (18), (19), and (20), we have used the specific form of the FDTD implementation proposed in the book by Gedney [76].

Mur ABC

In work [77], Mur has introduced a simple and convenient finite difference approximation for the second order Engquist-Majda ABC [78]:

$$\frac{\partial^2 E}{\partial x \partial t} - \frac{1}{c}\frac{\partial^2 E}{\partial t^2} + \frac{c}{2}\frac{\partial^2 E}{\partial y^2} + \frac{c}{2}\frac{\partial^2 E}{\partial z^2} = 0 \tag{21}$$

to be used specifically with the Cartesian Yee scheme [69]. The artificial boundary for (21) is x = const. Similar boundary conditions can be easily derived for other artificial boundaries, y = const and z = const. As of yet, we have implemented the Mur boundary conditions (21) at the faces of the computational domain, while at the edges and corners we have used the Sommerfeld ABC (18), as proposed in [76]. This approach leads to significant reflection errors, so at a later stage we plan to improve the implementation of (21) by employing the one-sided second order differences near edges and corners.

Numerical Experiments with Low Order ABCs

We started testing the foregoing local low order ABCs in the capacity of a standalone closure for the original problem, *i.e.*, without the lacunae-based time marching. For the Higdon ABC (19) and Betz-Mittra ABC (20) we took the values of $\phi_1 = 0$ and $\phi_2 = \pi/4$. In general, low order ABCs are expected to produce fairly significant spurious reflections from the artificial outer boundary back to the computational domain. The level of those reflections depends on the design of a given ABC, as well as on how close the artificial boundary is placed to the source of electromagnetic radiation.

In Figure 4, we are showing the profiles of the relative error for the various ABCs on the domain of size 5 discretized by the grid of dimension $30 \times 30 \times 30$ nodes. The plots demonstrate that the type of the ABC strongly affects the accuracy of computation. The highest level of error is generated by the Sommerfeld ABC (18), and the best ABC in this experiment is the Betz-Mittra ABC (20), yet even this ABC still yields a lager error than that of the PML [68].

In Figure 5, we are showing similar results but for the domain which is twice as large (size 10) and discretized by the grid of dimension $60 \times 60 \times 60$. In other words, while leaving the effect of the discretization the same, we are placing the outer boundary further away from the waves' source. By comparing the results in Figure 5 with those in Figure 4 we see that for the larger domain (Figure 5) all the error profiles, including that for the PML [68], have reached the same bottom (although the least accurate Sommerfeld ABC (18) still generates the highest peaks). This indicates that for the setting of Figure 5, the overall accuracy is dominated by the discretization error on the grid, whereas the reflection error due to the ABCs has decreased because the computational domain has become larger.

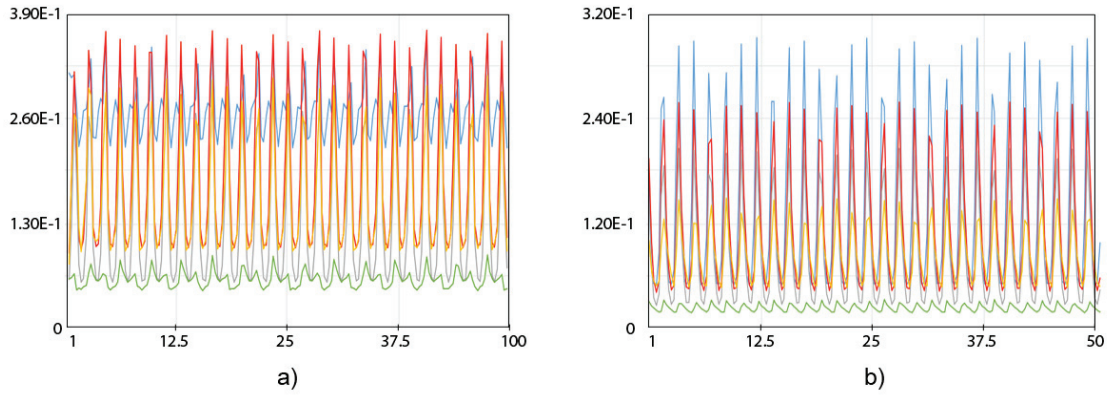

FIGURE 4. Relative error *vs.* time for the field components E_y (a) and H_x (b). The size of the computational domain in each direction is 5, and the grid dimension is $30 \times 30 \times 30$. Blue curve — Sommerfeld ABC (18), red curve — Higdon ABC (19), yellow curve — Mur ABC (21), grey curve — Betz-Mittra ABC (20), green curve — 15 point unsplit PML of [68]

Given that the error for the larger domain has reached the limit imposed by the discretization, we next study the grid convergence (see Figure 5), *i.e.*, refine the grid while keeping the domain size (equal to 10) and the ABCs

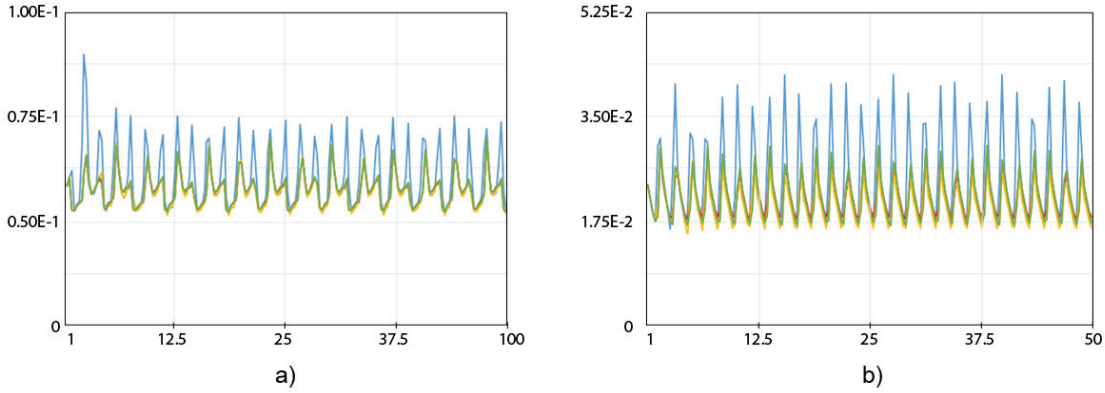

FIGURE 5. Relative error *vs.* time for the field components E_y (a) and H_x (b). The size of the computational domain in each direction is 10, and the grid dimension is $60 \times 60 \times 60$. Blue curve — Sommerfeld ABC (18), red curve — Higdon ABC (19), yellow curve — Mur ABC (21), grey curve — Betz-Mittra ABC (20), green curve — 15 point unsplit PML of [68]

the same. The results are presented in Figure 6. We see that the Sommerfeld ABC (18), as well as the Mur ABC (21) (which still uses the Sommerfeld ABC at the edges and corners of the domain) demonstrate practically no grid convergence at all. This means that when the grid is refined and the discretization error decreases, the overall error for these boundary conditions is dominated by reflections that are independent of the discretization. The best grid convergence is demonstrated by the Betz-Mittra ABC (20), but it still flattens after the first refinement of the grid. This means that on finer grids the reflection error again becomes dominant. The error behavior for the Higdon ABC (19) is similar to that of the Betz-Mittra ABC (20) albeit the overall convergence is somewhat slower. The unsplit PML of [68] shows robust grid convergence on the entire sequence of grids.

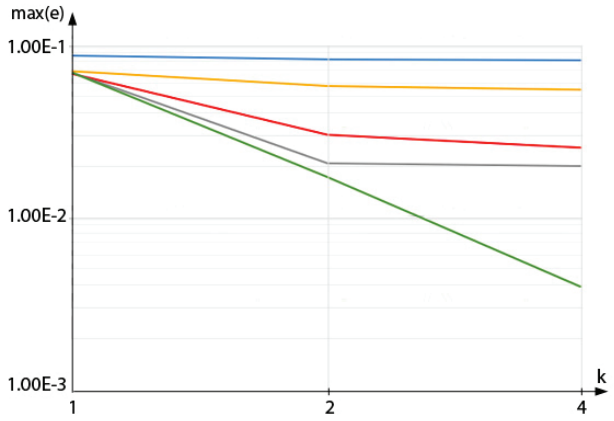

FIGURE 6. The grid convergence on the domain of size 10 for the field component E_y. The coarsest grid dimension is $60 \times 60 \times 60$; subsequent grids are refined by a factor of k, where $k = 2, 4$. Blue curve — Sommerfeld ABC (18), red curve — Higdon ABC (19), yellow curve — Mur ABC (21), grey curve — Betz-Mittra ABC (20), green curve — 15 point unsplit PML of [68]

Accuracy and Stability of Low Order ABCs

The two main components of numerical error in our simulations are due to the discretization on the grid and due to the reflections from the artificial outer boundary. Those two components are independent from one another and controlled by different factors: the grid size and the type of ABC/location of the boundary, respectively. The overall accuracy of computations provided by low order local ABCs is typically not very high because of a substantial level of reflections

from the outer boundary. Even the best performing ABC out of those we have considered (the Betz-Mittra ABC (20)) still appears inferior to the PML.

On the other hand, in those numerical experiments that we have conducted, we did not observe any long time deterioration of performance. In other words, the solution obtained with the help of low order local ABCs is stable yet not very accurate. The performance of local low order ABCs was compared against that of the unsplit PML [68]. For those simulation regimes that we have chosen, the PML did not show any long time deterioration either,[3] yet has overperformed the low order ABC from the standpoint of accuracy.

Most likely, local low order ABCs will not require any lacunae-based stabilization as their performance does not seem to deteriorate over long simulation times. However, the accuracy that they provide is not satisfactory. Therefore, our next steps are related to high order ABCs in several CEM codes.

Lacunae-based Stabilization of the PML in the OVERURE Toolkit

`OVERTURE` is a toolkit for solving partial differential equations on structured, overlapping, and hybrid grids. It provides a high level C++ interface for rapid prototyping of PDE solvers built upon optimized C and Fortran kernels, a library of finite-difference operators: conservative and non-conservative, 2nd, 4th, 6th and 8th order accurate approximations, and support for block structured adaptive mesh refinement (AMR). `OVERTURE` has extensive grid generation capabilities, CAD interfaces, interactive graphics and data base support, command scripts with embedded Perl commands. PDE solvers built upon `OVERTURE` include CGMX — a time domain Maxwell's equations solver, see [79], CGMP — a multi-physics solver, and others.

Governing Equations

The original first order Maxwell system of equations can be reduced to decoupled second order equations for the electric and magnetic field. The equation for the electric field reads:

$$\varepsilon\mu\partial_t^2 \boldsymbol{E} = \Delta \boldsymbol{E} + \nabla\left(\nabla \ln\varepsilon \cdot \boldsymbol{E}\right) + \nabla \ln\mu \times \left(\nabla \times \boldsymbol{E}\right) - \nabla\left(\frac{1}{\varepsilon}\rho\right) - \mu\partial_t \jmath, \tag{22}$$

where ε is the electric permittivity, μ is the magnetic permeability, $\jmath$ is the density of the extraneous electric current and ρ is the density of the electric charge. These quantities are related to one another via the continuity equation:

$$\frac{\partial\rho}{\partial t} + \operatorname{div}\jmath = 0.$$

For all our simulations, we use $\varepsilon = 1$ and $\mu = 1$, so Eq. (22) takes the form of the standard three-dimensional wave (d'Alembert) equation:

$$\partial_t^2 \boldsymbol{E} = \Delta \boldsymbol{E} + \boldsymbol{F} \tag{23}$$

driven by the external source:

$$\boldsymbol{F} = -\nabla\rho - \partial_t \jmath. \tag{24}$$

We have conducted two types of numerical experiments done on the basis of Eq. (b)):

- Type I experiment: Simulation of the electromagnetic field generated in vacuum by a given current $\jmath$ and its respective charge ρ (*e.g.*, antenna with a given feed). The computational domain is terminated by a PML combined with the lacunae-based time marching.
- Type II experiment: Simulation of the scattering of a given impinging plane electromagnetic wave about an object of a given composition and shape. The simplest scatterer is a perfectly conducting sphere. No extraneous currents are present. Again, the computational domain is terminated by a PML combined with the lacunae-based time marching.

[3] There are many cases for which the PML performs well altogether; otherwise, even if an instability develops it may manifest itself only after a rather long period of satisfactory performance.

Type I Experiment Results

To assess the performance of the lacunae-based algorithm in Type I experiments, we use a reference solution in the form of a propagating TM-mode of electromagnetic field. Its non-zero components in the spherical coordinates are:

$$E_r(r,\theta,t) = \psi(r)\frac{2d_0\cos\theta}{r^3}\left(\chi + \frac{\dot\chi r}{c}\right) - \frac{d_0\cos\theta}{r^2}\left(\chi + \frac{\dot\chi r}{c} + \frac{\ddot\chi r^2}{c^2}\right)\frac{\partial\psi}{\partial r}, \tag{25}$$

$$E_\theta = \psi(r)\frac{d_0\sin\theta}{r^3}\left(\chi + \frac{\dot\chi r}{c} + \frac{\ddot\chi r^2}{c^2}\right), \tag{26}$$

$$H_\varphi = \psi(r)\frac{d_0\sin\theta}{cr^3}\left(\dot\chi r + \frac{\ddot\chi r^2}{c}\right), \tag{27}$$

where

$$\psi(r) = 1 - e^{-\alpha r^6}, \tag{28}$$

$$\chi(t - r/c) = \sin^4[\omega_1(t - r/c)] + \sin^4[\omega_2(t - r/c)], \tag{29}$$

and the upper dot denotes differentiation with respect to t. The fields (25)-(27) are generated by the following non-zero components of the electric current:

$$j_r = \frac{d_0\cos\theta}{cr^2}\left(\dot\chi + \frac{\ddot\chi r}{c} + \frac{\dddot\chi r^2}{c^2}\right)\frac{\partial\psi}{\partial r}, \tag{30}$$

$$j_\theta = -\frac{d_0\sin\theta}{cr^3}\left(\dot\chi r + \frac{\ddot\chi r^2}{c}\right)\frac{\partial\psi}{\partial r}. \tag{31}$$

The forcing term $\boldsymbol{F}$ of (24) also involves the electric charge ρ which is obtained by integration of the currents:

$$\rho = -\frac{\cos\theta}{r^3}\left[\left(r\frac{\partial^2\psi}{\partial r^2} - 2\frac{\partial\psi}{\partial r}\right)(r\dot\chi + \chi) + \left(r^3\frac{\partial^2\psi}{\partial r^2} + \frac{\partial\psi}{\partial r}\right)\ddot\chi + r^3\frac{\partial\psi}{\partial r}\dddot\chi\right]. \tag{32}$$

The factor $\psi(r)$ of (28) is $O(r^6)$ as $r \to 0$ and suppresses all the singularities that may appear in the functions (25)-(27) and (30)-(32) at $r = 0$. On the other hand, the derivatives $\frac{\partial\psi}{\partial r}$ and $\frac{\partial^2\psi}{\partial r^2}$ decay very rapidly for large r which effectively implies $\boldsymbol{F} = \boldsymbol{0}$ (to machine precision) sufficiently far away from the origin. By appropriately choosing the parameter α one can ensure that $\mathrm{supp}\boldsymbol{F} \subseteq S_0$, where S_0 is a given bounded domain that contains the origin and $\mathrm{supp}\boldsymbol{F}$ is the set where $\boldsymbol{F} \neq \boldsymbol{0}$. We also note that the solution (25)-(27) is a regularized (at $r = 0$) version of the field radiated by the elementary dipole $d(t) = d_0\chi(t)$ located at the origin and aligned with the z-axis.

In Figure 7, we compare two types of boundary closure for the problem: (i) the pure PML approach when the problem is integrated on the domain S_{aux} which is truncated by means of the PML with no use of no lacunae and (ii) the lacunae-based algorithm combined with the same PML. The parameters of the PML are the same in both cases. Figure 7 clearly indicates the pure PML approach leads to an abrupt divergence after a relatively short period of stable behavior. The error in Figure 7 is bounded by 1 because we use the computed solution rather than the reference solution in the denominator. The computed solution $E_{i,j,k}$ itself tends to infinity, *i.e.*, blows up, in this situation. Yet the lacunae-based algorithm provides a perfect correction for the instability developing in the PML. The computational time T in these runs corresponds to about 120 diameters of S. Over this time, about 60 partial APs were "recycled."

In Figure 8, we demonstrate the second order grid convergence of the algorithm that involves the lacunae-based integration combined with the PML.

So far, the lacunae-based methodology has been able to stabilize the long-time behavior of a given boundary procedure, which demonstrates both its universality and consistent performance.

Type II Experiment with External Scattering by Sphere

We consider external scattering by perfectly electrically conducting (PEC) bodies. For our simulations we choose two scattering shapes. The first one is a sphere, and the second one is a geometrically more complex body of revolution that schematically represents a reentry vehicle.

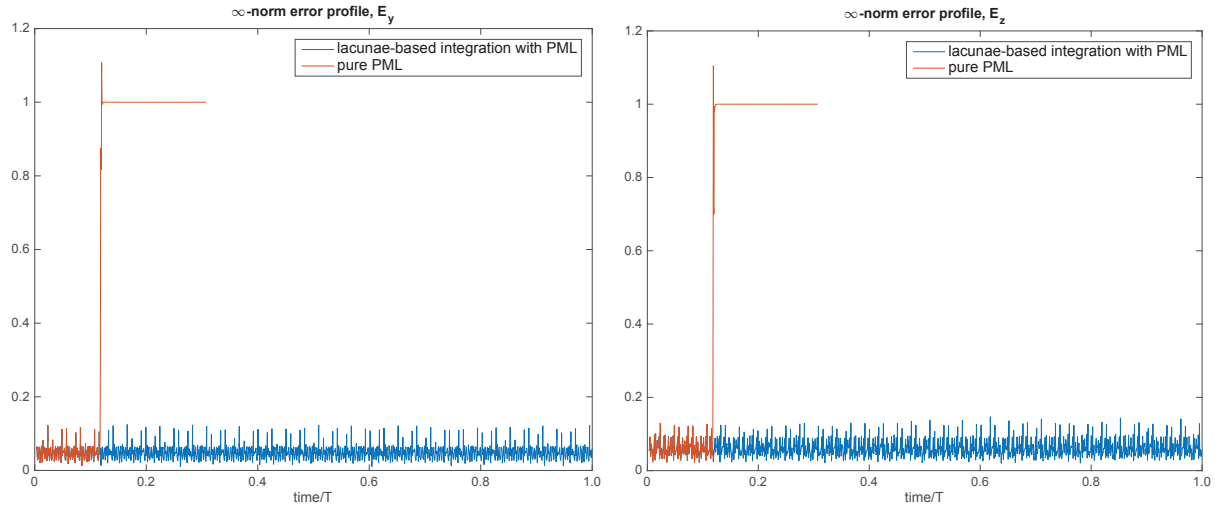

FIGURE 7. Left: error profile of E_y (∞-norm) computed under the pure PML approach and the lacunae-based integration. Right: the same for E_z. The pure PML ABC solution starts diverging exponentially at time $t > 0.5$ (red curve), while lacuna-based solution (blue curve) remains stable and accurate

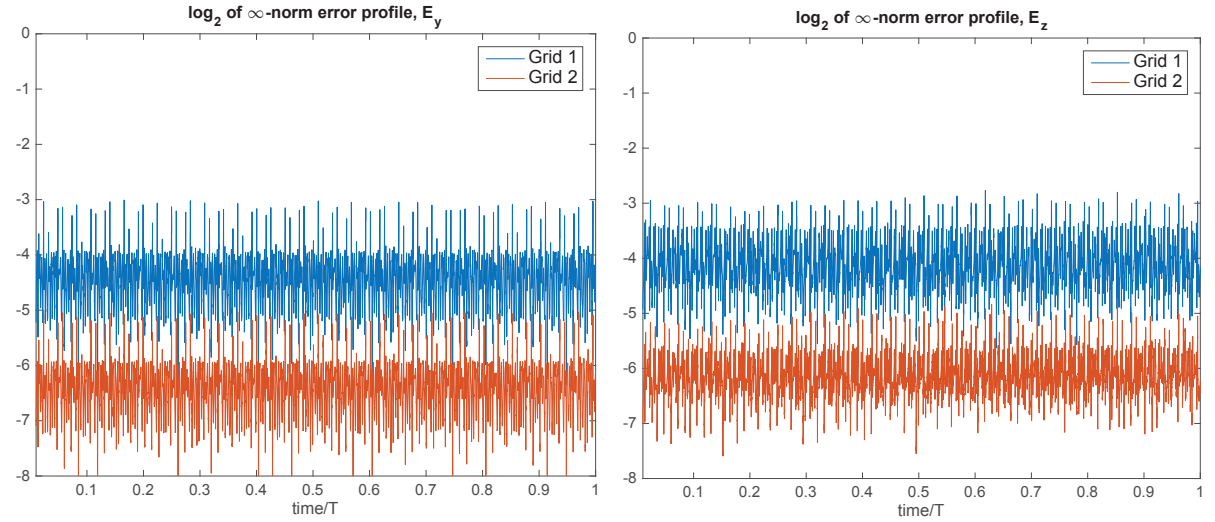

FIGURE 8. Demonstration the second order grid convergence of the algorithm. Left: error profiles for E_y (binary logarithm of ∞-error norm) on two successive grids. Right: the same for E_z

The excitation in the scattering problems is provided by a given impinging wave. It is taken in the form of a linearly polarized (along the y axis) monochromatic transverse plane wave of unit amplitude:

$$\boldsymbol{E} = \mathbf{e}_y \cos(\omega t - kx). \tag{33}$$

For $k > 0$, the wave (33) propagates in the positive x direction. The wavelength in (33) is assumed equal to one. The characteristic size of both scattering shapes that we are going to consider, the sphere and the reentry vehicle, will also be of order one. This rules out the use of any asymptotic solutions (either the geometrical optics for short waves or the diffraction of long waves on a small obstacle) and requires a direct numerical simulation of the scattered field.

The PEC sphere of radius one is embedded into the domain S and centered at the origin, see Figure 9. The scattering process is modeled by imposing the PEC boundary conditions on the sphere, which is done by a special built-in subroutine in `OVERTURE`. The PEC boundary conditions require that the tangential component of the electric

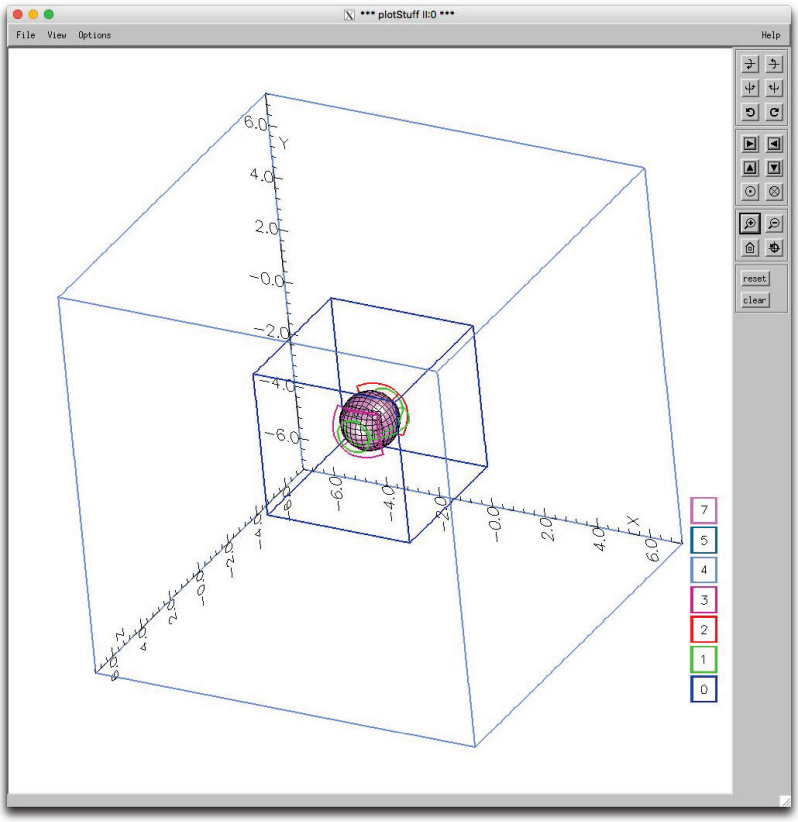

FIGURE 9. Computational domains for the sphere

field be equal to zero. The initial conditions are taken homogeneous for simplicity. This is inconsistent with the boundary data. Hence, we expect to see a transition period in the simulations, after which the solution will go into a harmonic oscillation mode.

It is important to note that the overlapping grids that we employ to discretize the sphere may lead to an unstable behavior of the algorithm even in its original setting, *i.e.*, before we add any lacunae-based routines. To suppress the instability, `OVERTURE` introduces artificial dissipation, which is generally small and can be controlled by the user. In Figure 10, we demonstrate the unstable behavior at zero artificial dissipation with or without the lacunae-based integration. Specifically, we show the reflected field at the spatial location $(-2.5, 0, 0)$ in front of the sphere. After a short period of stable performance, it begins to grow rapidly, which is a clear indication of instability.

In Figure 11, we demonstrate the instability that develops in this scattering problem when the PML is used as the only means for truncating the computational domain, *i.e.*, without the lacunae-based time marching. The strength of the PL is taken as $A = 83$. In the same figure, we present the results for the combined lacunae+PML approach, which clearly removes the blow-up behavior. To corroborate that the performance remains stable over long times, we run the same lacunae+PML computation ($A = 83$) for the total time T that corresponds to about 120 diameters of S. The results are presented in Figure 12. We observe stable oscillations with no signs of divergence.

In Figure 13, we are showing a 3D plot of the scattered field at the moment of time $t = 0.03T$, where T is large, about 120 diameters of S. This time is beyond the initial period of transient behavior. The plane wave impinges on the sphere from the right along the x axis. The actual plot shown in Figure 13 was done in MATLAB using the numerical data saved in `OVERTURE`.

Experiment with External Scattering by Reentry Vehicle

Next, we describe another Type II experiment: numerical simulation of the scattering of a plane impinging wave about a PEC body of revolution that represents a model reentry vehicle, see Figure 14(b).

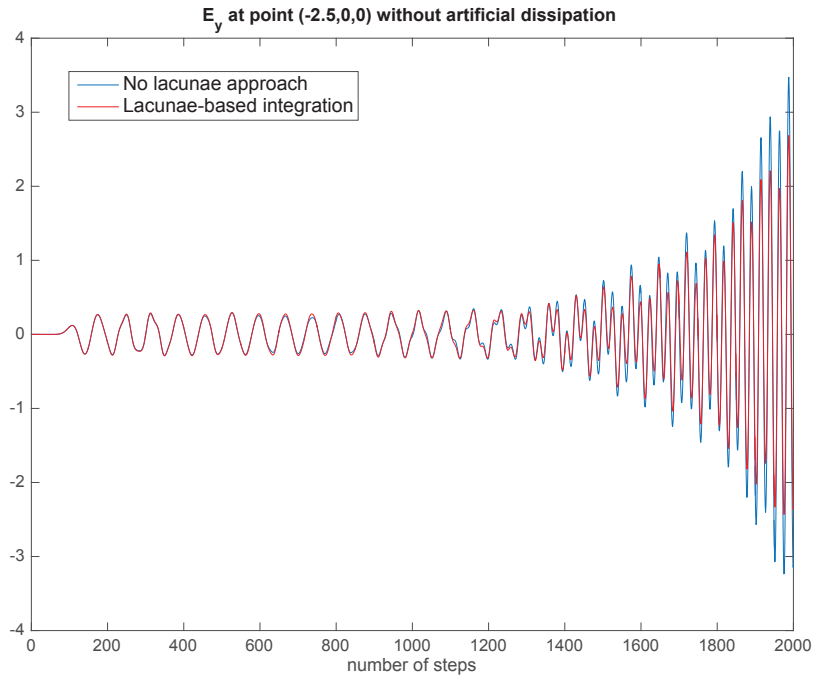

FIGURE 10. The reflected field E_y at the point $(-2.5, 0, 0)$ in the absence of artificial dissipation

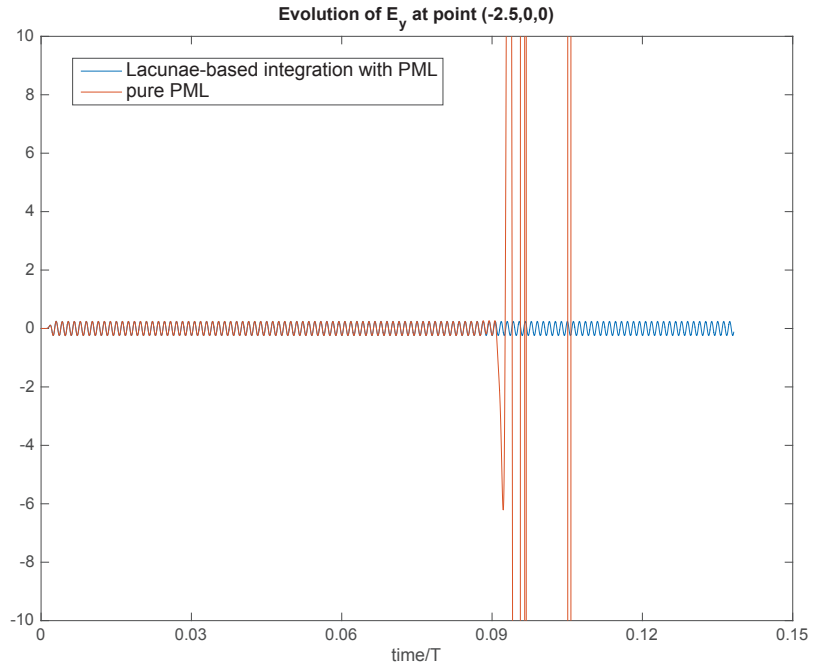

FIGURE 11. The reflected field E_y at the location $(-2.5, 0, 0)$. Pure PML and the combined PML+lacunae approach

The computational setup is schematically shown in Figure 14(b). The domain S is defined as a box with dimensions $[-4, 5]\times[-4, 5]\times[-4, 5]$; it is discretized by a $61\times61\times61$ grid. The auxiliary domain S_{aux} is a box of dimension $[-8, 10] \times [-8, 10] \times [-8, 10]$ discretized by a $121 \times 121 \times 121$ grid. Inside S, there is a body of revolution built with

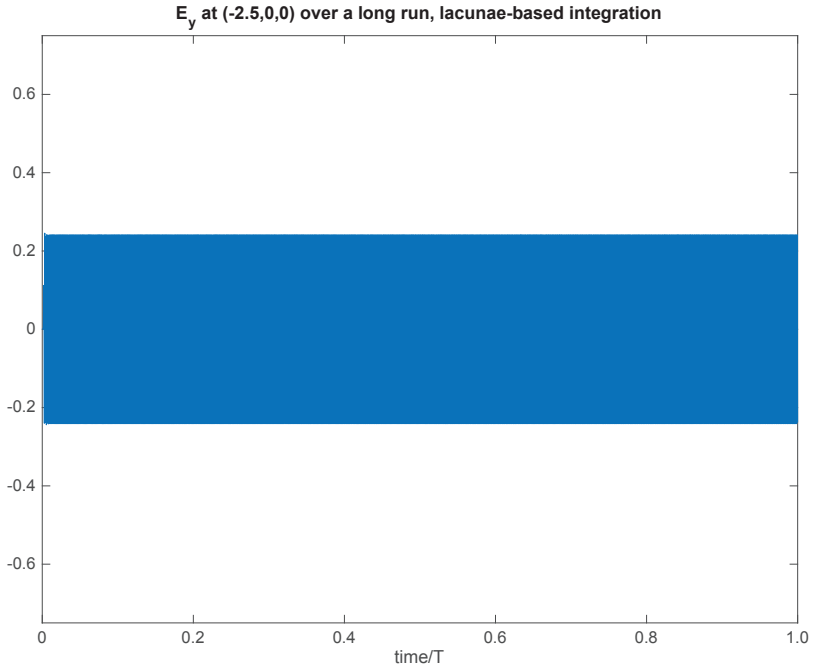

FIGURE 12. The reflected field E_y at the location $(-2.5, 0, 0)$ over a long run. Lacunae-based integration combined with the PML

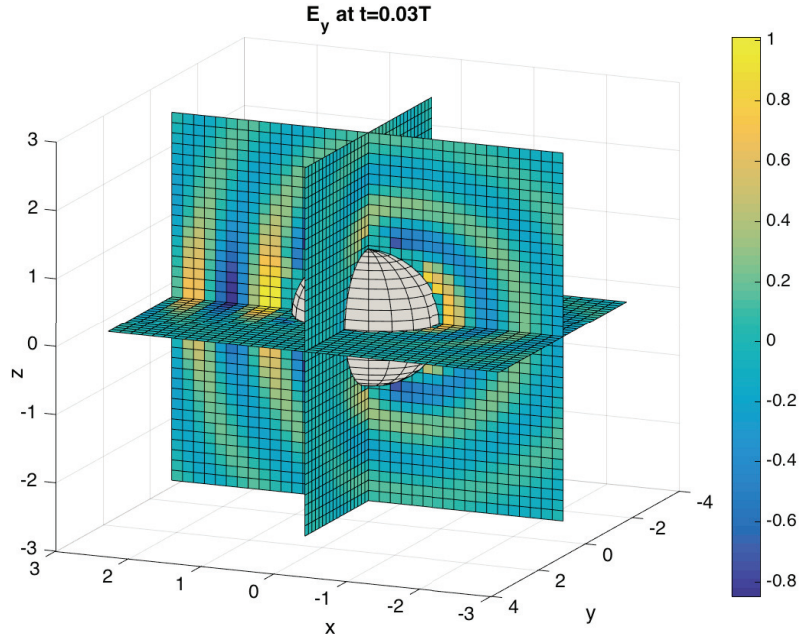

FIGURE 13. Scattered field E_y on S at the time $t = 0.03T$

the help of the appropriate OVERTURE tools and discretized by means of the overlapping grids, see Figure 14(b). The domain S is not centered at the origin because the scatterer is displaced from zero along the x-axis (under the current implementation of this object in OVERTURE).

A monochromatic plane wave of unit wavelength impinges on the body from the right, *i.e.*, $k = -2\pi$ in formula

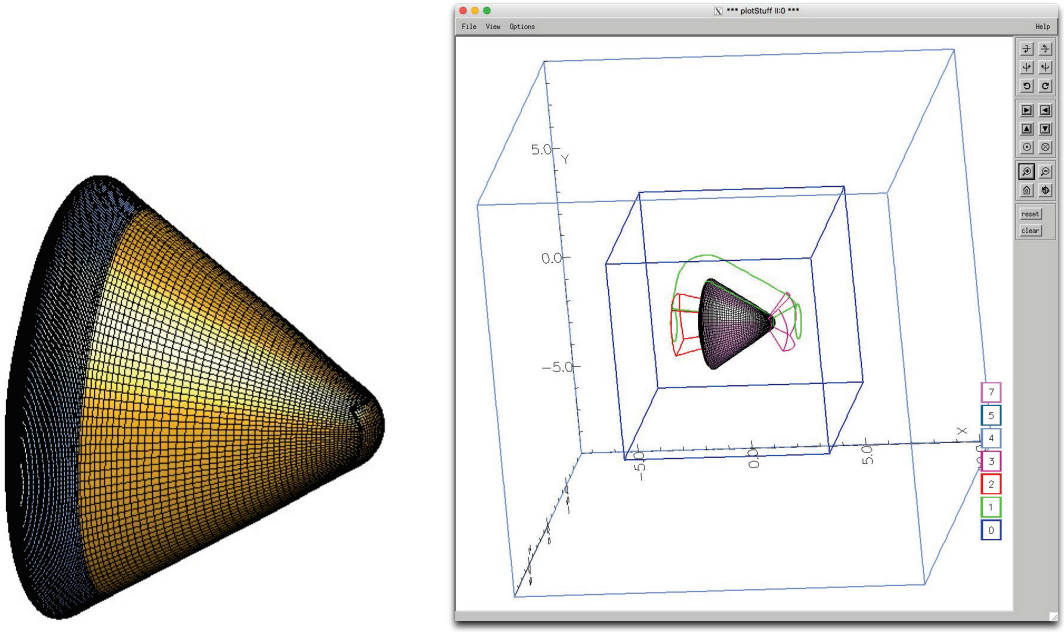

(a) (b)

FIGURE 14. Reentry vehicle: (a) Geometry. (b) Computational domain for the reentry vehicle

(33) so that the wave travels in the negative x direction. This plane wave is polarized along the y axis. As before, the artificial dissipation is introduced only near the scatterer rather than on the entire domain S. A 25-node PML is set at the artificial outer boundary; the strength of the PML is $A = 58$. The evolution of the E_y component of the electric field is shown in Figure 15. Emergence of an instability in electromagnetic wave scattering of a plane wave by a model reentry vehicle is observed with time.

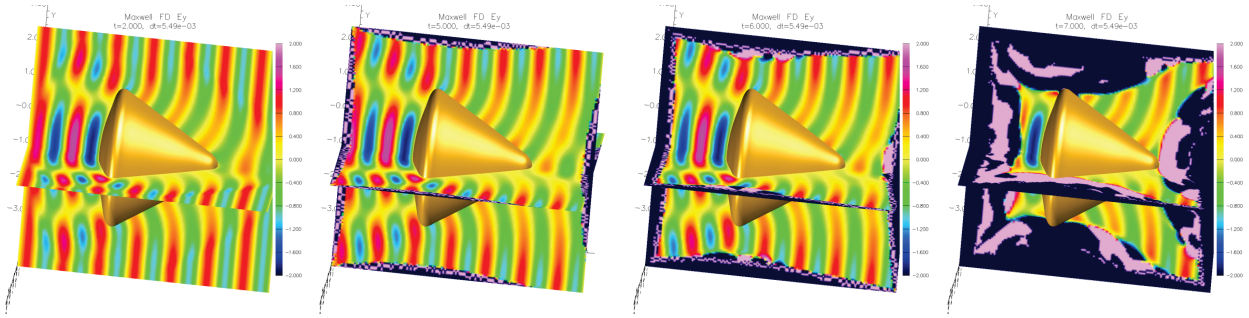

FIGURE 15. Emergence of an instability in electromagnetic wave scattering of a plane wave by a model reentry vehicle. Snapshots of E_y shown in two planes are taken at a sequence of simulation times from $time/T = 0.05$ to $time/T = 0.13$

Simulations result in a sharp instability at rather small time, $t > 0.12$ for the pure PML (red curve), as indicated by the temporal profile of the scattered component E_y shown in the left panel of Figure 16. Even with the PML+Lacuna (blue curve) profile blows up after $t = 0.35T$, which is typical for a developing numerical instability.

Of course, to be able to attribute the instability unambiguously to a given cause, *e.g.*, to the overlapping grids, one needs to rule out other possible causes, in particular, to eliminate the influence of the artificial outer boundary.

To do so, *i.e.*, to make sure that it is not the lacunae-based time marching that is causing the instability, we performed the same computation in the genuine `OVERTURE` framework using the Engquist-Magda artificial boundary conditions at ∂S.

The artificial dissipation was applied on the entire domain S. In these computations, we observed exactly the same

behavior as that of the blue curve in the left panel of Figure 16 — a blowup of the solution shortly after $t = 0.35T$. This suggests that the instability is, in fact, induced by the overlapping grids that discretize the scatterer rather than by the treatment of the artificial outer boundary.

Of course, it is entirely possible that this instability could be reduced or eliminated by adjusting the artificial dissipation. This, however, would require an additional thorough numerical investigation that we have not performed.

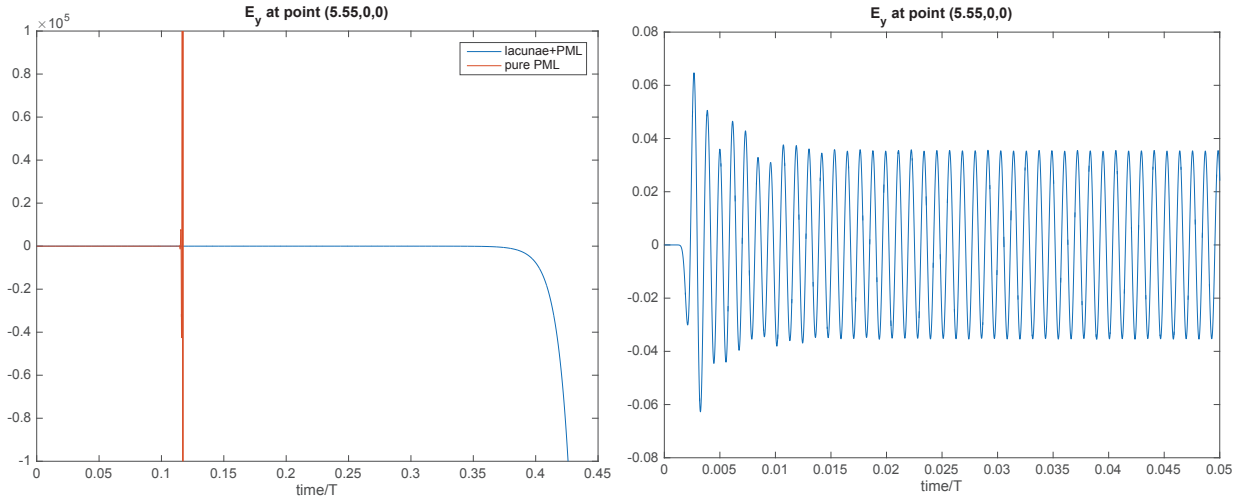

FIGURE 16. Left: Scattered field E_y vs time. Pure PML and lacunae+PML approaches are presented. Pure PML results in an instability. Right: Zoom in for an early stage of the evolution of E_y

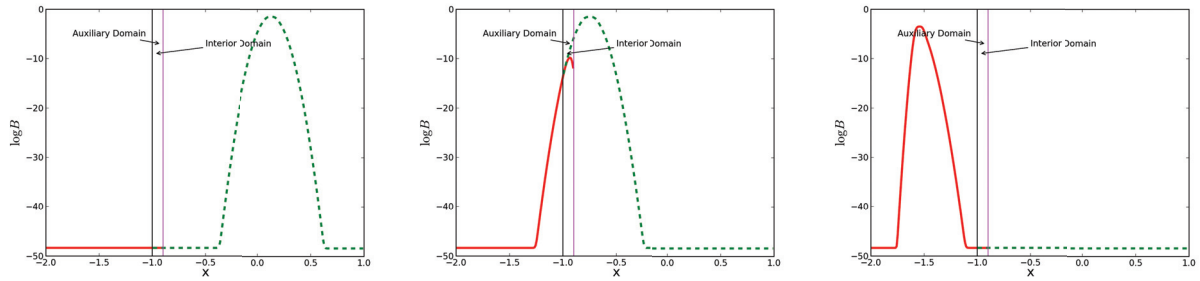

FIGURE 17. Demonstration of 1D electromagnetic pulse propagating through ABC without reflections in the finite volume version of `WARPX`: (a) $t = 10$, (b) $t = 20$, (c) $t = 30$

Instead, we compare the performance of the pure PML closure at the artificial outer boundary against that of the lacunae+PML approach over the interval of time for which the foregoing interior instability does not manifest itself yet. Figure 16 clearly demonstrates that the solution terminated by the PML itself blows up fairly early on, whereas the lacunae-based time marching combined with the PML eliminates this blowup and maintains stable performance, as expected by design. This stable performance is later disrupted by the instability which develops due to the overlapping grids and thus cannot be cured by employing an alternative treatment of the artificial outer boundary.

Numerical Computations Using the Code `WARPX`

Lacunae-based boundary conditions have been implemented in `WARPX`[80] using a finite volume spatial discretization. Since `WARPX` models plasma dynamics using a multi-fluid plasma model coupled with Maxwell's equations, it is

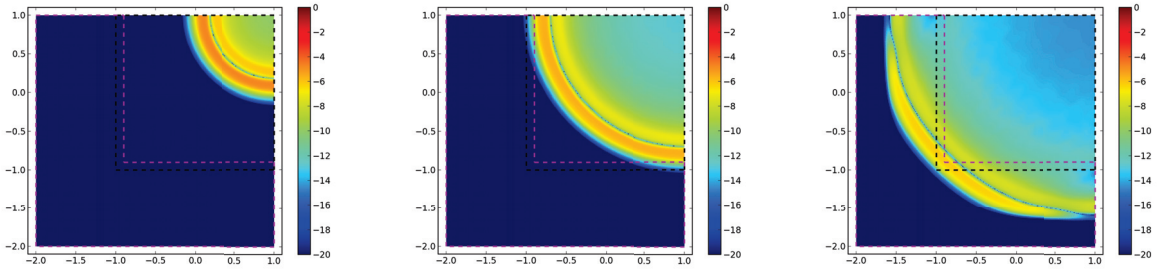

(a) (b) (c)

FIGURE 18. Demonstration of 2D electromagnetic pulse propagating through ABC without reflections in the finite volume version of WARPX. Shown are contours of $\log|B_z|$: (a) $t = 10$, (b) $t = 20$, (c) $t = 30$

essential that light waves exit the truncated computational domain without causing artificial reflections at the boundaries. The performance of the ABC is demonstrated by launching an electromagnetic pulse towards a boundary and observing any reflected waves. One-dimensional results are shown in Figure 17 where the out-of-plane component of the magnetic field (B_z) is seen to propagate through the open boundary at $x = -1$ without producing reflections. The ABC also performs well in two-dimensional geometries where no true lacunae are expected. Figure 18 shows the results for a cylindrical electromagnetic pulse passing through an open BC on the lower and left boundaries.

CONCLUSIONS

Altogether, we have conducted an extensive series of lacunae-based numerical experiments using several different codes (an in-house FDTD Yee code, OVERTURE, and WARPX), and various options for the treatment of artificial boundaries. The results convincingly demonstrate ***the feasibility, efficiency, and versatility of the proposed lacunae-based methodology*** as a technique for building the non-deteriorating boundary conditions in CEM. The methodology can also be combined with the interior solvers developed by other parties.

We conclude that ***the lacunae-based approach removes a key difficulty that currently hampers many existing methods for computing unsteady electromagnetic waves on unbounded regions.***

The algorithm provides a temporally uniform guaranteed error bound (no deterioration in most cases), and the software will enable robust electromagnetic simulations in a high-performance computing environment.

ACKNOWLEDGEMENTS

Work supported by the US Army Phase II STTR contract W911NF-14-C-0161; Program manager Dr. Joe Myers.

REFERENCES

[1] J.-P. Bérenger (1994) *J. Comput. Phys.* **114**, 185.
[2] J.-P. Bérenger (1996) *J. Comput. Phys.* **127**, 363.
[3] S. D. Gedney (1996) *IEEE Trans. Antennas Propagat.* **44**, 1630.
[4] R. W. Ziolkowski (1997) *IEEE Trans. Antennas Propagat.* **45**, 1530.
[5] S. Abarbanel and D. Gottlieb (1998) *Appl. Numer. Math.* **27**, 331.
[6] S. Abarbanel and D. Gottlieb (1997) *J. Comput. Phys.* **134**, 357.
[7] S. Abarbanel, D. Gottlieb, and J. S. Hesthaven (2002) *J. Sci. Comput.* **17**, 405.
[8] J. Diaz and P. Joly (2006) *Comput. Methods Appl. Mech. Engrg.* **195**, 3820.
[9] O. M. Ramahi (1999) *IEEE Trans. Antennas Propagat.* **47**, 593.
[10] J. Diaz and P. Joly (2005) *SIAM J. Appl. Math.* **65**, 1547.
[11] T. Hagstrom and T. Warburton (2009) *SIAM J. Numer. Anal.* **47**, 3678.
[12] B. Alpert, L. Greengard, and T. Hagstrom (2000) *SIAM J. Numer. Anal.* **37**, 1138.

[13] B. Alpert, L. Greengard, and T. Hagstrom (2002) *J. Comput. Phys.* **180**, 270.
[14] C. Lubich and A. Schädle (2002) *SIAM J. Sci. Comput.* **24**, 161.
[15] T. Hagstrom and S. Lau (2007) *J. Comput. Math.* **25**, 305.
[16] R. L. Higdon (1987) *Math. Comp.* **49**, 65.
[17] R. L. Higdon (1986) *Math. Comp.* **47**, 437.
[18] A. Taflove and S. C. Hagness, *Computational Electrodynamics: the Finite-Difference Time-Domain Method*, 3rd edn. (Artech House Inc., Boston, MA, 2005).
[19] R. L. Wagner and W. C. Chew (1995) *J. Electromagn. Waves Applicat.* **9**, 993.
[20] O. M. Ramahi (1995) *Microwave Opt. Technol. Lett.* **15**, 132.
[21] T. Hagstrom, T. Warburton, and D. Givoli (2010) *J. Comput. Appl. Math.* **234**, 1988.
[22] S. D. Gedney, "The perfectly matched layer absorbing medium," in *Advances in Computational Electrodynamics: The Finite-Difference Time-Domain Method*, edited by A. Taflove, (Artech House, Boston, MA, 1998), pp. 263–340.
[23] J. A. Roden and S. D. Gedney (2000) *Microwave and Optical Technology Letters* **27**, 334.
[24] E. Bécache, P. G. Petropoulos, and S. D. Gedney (2004) *IEEE Trans. Antennas and Propagation* **52**, 1335.
[25] S. Abarbanel, D. Gottlieb, and J. S. Hesthaven (2006) *J. Sci. Comput.* **28**, 125.
[26] I. Petrowsky (1945) *Matematicheskii Sbornik (Recueil Mathématique)* **17**(59), 289.
[27] V. S. Vladimirov, *Equations of Mathematical Physics* (Dekker, New-York, 1971).
[28] R. Courant and D. Hilbert, *Methods of Mathematical Physics. Vol. II* (Wiley, New York, 1962).
[29] J. Hadamard, *Lectures on Cauchy's Problem in Linear Partial Differential Equations* (Yale University Press, New Haven, 1923).
[30] J. Hadamard, *Problème de Cauchy* (Hermann et cie, Paris, 1932). [in French]
[31] J. Hadamard (1942) *Ann. of Math. (2)* **43**, 510.
[32] M. F. Atiyah, R. Bott, and L. Gårding (1970) *Acta Math.* **124**, 109.
[33] M. F. Atiyah, R. Bott, and L. Gårding (1973) *Acta Math.* **131**, 145.
[34] M. Matthisson (1939) *Acta Math.* **71**, 249. [in French]
[35] K. L. Stellmacher (1953) *Nachr. Akad. Wiss. Göttingen. Math. Phys. Kl. Math.-Phys. Chem. Abt.* **1953**, 133. [in German]
[36] J. E. Lagnese and K. L. Stellmacher (1967) *J. Math. Mech.* **17**, 461.
[37] K. L. Stellmacher (1955) *Math. Ann.* **130**, 219. [in German]
[38] R. Schimming, "A review of Huygens' principle for linear hyperbolic differential equations," in *Proc. of the IMU Symposium "Group-Theoretical Methods in Mechanics," Novosibirsk, USSR, 1978*, (Novosibirsk, USSR Acad. Sci., Siberian Branch, 1978).
[39] M. Belger, R. Schimming, and V. Wünsch (1997) *Z. Anal. Anwendungen* **16**, 9.
[40] P. Günther, *Huygens' Principle and Hyperbolic Equations*, volume 5 of *Perspectives in Mathematics* with appendices by V. Wünsch (Academic Press Inc., Boston, MA, 1988).
[41] P. Günther (1965) *Arch. Rational Mech. Anal.* **18**, 103. [in German]
[42] P. D. Lax and R. S. Phillips (1978) *Comm. Pure Appl. Math.* **31**, 415.
[43] S. V. Petropavlovsky and S. V. Tsynkov (2011) *SIAM J. Appl. Math.* **71**(4), 1109–1122.
[44] V. S. Ryaben'kii, S. V. Tsynkov, and V. I. Turchaninov (2001) *Appl. Numer. Math.* **38**, 187.
[45] V. S. Ryaben'kii, S. V. Tsynkov, and V. I. Turchaninov (2001) *J. Comput. Phys.* **174**, 712.
[46] S. V. Tsynkov (2003) *J. Comput. Phys.* **189**, 626.
[47] S. V. Tsynkov (2004) *J. Comput. Phys.* **199**, 126.
[48] H. Qasimov and S. Tsynkov (2008) *J. Comput. Phys.* **227**, 7322.
[49] S. V. Petropavlovsky and S. V. Tsynkov (2012) *J. Comput. Phys.* **231**(2), 558–585.
[50] A. F. Peterson, S. L. Ray, and R. Mittra, *Computational Methods for Electromagnetics* (Electromagnetic Wave Theory, IEEE Press, 1997).
[51] W. C. Chew, M. S. Tong, and B. Hu, *Integral Equation Methods for Electromagnetic and Elastic Waves* (Morgan and Claypool Publishers, 2007).
[52] H. Contopanagos, B. Dembart, M. Epton, J. J. Ottusch, V. Rokhlin, J. L. Visher, and S. M. Wandzura (2002) *IEEE Trans. on Antennas and Prop.* **50**, 1824.
[53] A. F. Peterson (1990) *Electromagnetics* **10**, 293.
[54] J. Nye (2003) *Journal of Physics A – Mathematical and General* **36**, 4221.
[55] F. P. Andriulli, A. Tabacco, and G. Vecchi (2007) *SIAM J. Sci. Comput.* **29**, 1.
[56] Y. Zhang, T. J. Cui, W. C. Chew, and J.-S. Zhao (2003) *IEEE Trans. on Antennas and Prop.* **51**, 1864.

[57] F. P. Andriulli, K. Cools, F. Olyslager, and E. Michielssen (2009) *IEEE Trans. on Antennas and Prop.* **57**, 2365.
[58] K. Cools, F. P. Andriulli, F. Olyslager, and E. Michielssen (2009) *IEEE Trans. on Antennas and Prop.* **57**, 2352.
[59] G. C. Hsiao and R. E. Kleinman (1997) *IEEE Trans. on Antennas and Prop.* **45**, 316.
[60] G. Vecchi (1999) *IEEE Trans. on Antennas and Prop.* **47**, 339.
[61] J. S. Zhao and W. C. Chew (2000) *IEEE Trans. on Antennas and Prop.* **48**, 1635.
[62] L. D. Landau and E. M. Lifshitz, *Course of Theoretical Physics, Vol. 2: The Classical Theory of Fields*, 4th edn. (Pergamon Press, Oxford, 1975).
[63] L. D. Landau and E. M. Lifshitz, *Course of Theoretical Physics., Vol. 8: Electrodynamics of Continuous Media* (Pergamon Press, Oxford, 1984).
[64] T. Hagstrom, M. L. De Castro, D. Givoli, and D. Tzemach (2007) *J. Comput. Acoust.* **15**, 1.
[65] T. Hagstrom, A. Mar-Or, and D. Givoli (2008) *J. Comput. Phys.* **227**, 3322.
[66] E. Bécache, D. Givoli, and T. Hagstrom (2010) *J. Comput. Phys.* **229**, 1099.
[67] E. Bécache and P. Joly (2002) *M2AN Math. Model. Numer. Anal.* **36**, 87.
[68] L. Zhao and A. C. Cangellaris (1996) *IEEE Trans. Microwave Theory Tech.* **44**, 2555.
[69] K. S. Yee (1966) *IEEE Trans. Antennas Propagat.* **14**, 302.
[70] S. A. Schelkunoff (1936) *Bell System Technical Joirnal* **15**, 92.
[71] J.-P. Bérenger (2006) *IEEE Trans. Ant. Propag.* **54**, 3797.
[72] J.-P. Bérenger (2007) *J. Comput. Phys.* **226**, 354.
[73] W. D. Henshaw (2006) *SIAM J. Sci. Comput.* **28**, 1730.
[74] V. Betz and R. Mittra (1992) *IEEE Microwave and Guided Wave Letters* **2**(12), 499–501.
[75] V. Betz and R. Mittra (1993) *IEEE Microwave and Guided Wave Letters* **3**(6), 182–184.
[76] S. D. Gedney, *Introduction to the Finite-Difference Time-Domain (FDTD) Method for Electromagnetics* (Morgan & Claypool Publishers, San Rafael, CA, 2011).
[77] G. Mur (1981) *IEEE Trans. Electromagnetic Compatibility* **23** 377–382.
[78] B. Engquist and A. Majda (1977) *Math. Comp.* **31**(139), 629–651.
[79] W. D. Henshaw (2006) *SIAM J. Sci. Comput.* **28**, 1730.
[80] U. Shumlak, R. Lilly, N. Reddell, E. Sousa, and B. Srinivasan (2011) *Computer Physics Communications* **182**, 1767.